CrossMark

Selective hydrogenation of furfuryl alcohol to tetrahydrofurfuryl alcohol over Ni/γ-Al$_2$O$_3$ catalysts

Shengya Sang[1] · **Yuan Wang**[1] · **Wei Zhu**[1] ·
Guomin Xiao[1]

Abstract A series of nickel-based catalysts (with <5 nm Ni particle size) with γ-alumina as a support (x wt% Ni/γ-Al$_2$O$_3$, x represents the Ni loading amount) were synthesized by the impregnation method, which was successfully applied for the catalytic hydrogenation of furfuryl alcohol to tetrahydrofurfuryl alcohol. The effects of reaction time, reaction temperature, nickel loading amount, solvent, and hydrogen pressure on conversion of furfural alcohol as well as selectivity for tetrahydrofurfuryl alcohol were investigated systematically. The conversion of furfural alcohol over 15 wt% Ni/γ-Al$_2$O$_3$ was up to 99.8 % with a selectivity of 99.5 % toward tetrahydrofurfuryl alcohol, when the reaction was carried out at 353 K with an initial H$_2$ pressure of 4.0 MPa and reaction time of 2 h. In addition, there was an increase of turnover frequency (TOF) value with the decrease of Ni particle size. The features of the Ni/γ-Al$_2$O$_3$ catalysts were investigated by characterization of XRD, TPR, BET, and SEM.

Introduction

Recently, with the development of the economy and the decrease of petroleum reserves, researchers have realized that renewable energy is of great importance for sustainable development. Biomass was regarded as significant substitute goods for the production of fuels and chemicals [1–4]. Furfural (FFR) is one kind of important platform compound derived from biomass, which is contained in the hemicellulose

✉ Guomin Xiao
  xiaogm426@gmail.com

[1] School of Chemistry and Chemical Engineering, Southeast University,
  Nanjing 211189, Jiangsu, China

⌷ Springer

part of lignocellulosic biomass [5–10]. The FFR contains both C=O and C=C double bonds and with hydrogenation of FFR, it can produce a series of downstream compounds such as furfuryl alcohol (FA), tetrahydrofurfural, and tetrahydrofurfuryl alcohol (THFA) [11]. Yoshinao Nakagawa et al. [11–13] also reported about FFR concerning the conversion of FFR to tetrahydrofurfuryl alcohol (THFA) with silica-support nickel catalyst. In some reports, they also report about conversion of FFR to 1,5-pentanediol (1,5-PeD) [14, 15].

Furfuryl alcohol (FA) is a downstream product of furfural [16], which can be obtained by selective hydrogenation of FFR, and the catalyst has been successfully industrialized. Tetrahydrofurfuryl alcohol (THFA) is an important downstream product of FA, which is an important organic solvent, and is widely used in the industrial and agricultural fields [17, 18]. Because of its benign nature and low toxicity, it is also widely used as resin in the industry. THFA can be also obtained from the direct hydrogenation of FFR [19, 20]. Many other different useful chemicals can be also produced from THFA, such as δ-valerolactone [21, 22], tetrahydrofuran [22–25], and 4-penten-1-ol [21, 26–28]. Koso et al. [29, 30] and Nakagawa et al. [31–33] have reported that the conversion of THFA to 1,5-pentanediol (1,5-PeD) with different support catalysts and the selectivity of 1,5-PeD of up to 70 %. In their reports, two steps were reported about the conversion of THFA to 1,5-PeD [34, 35]. A multi-step method was proposed by Schniepp's [34] team, but this method needs the isolation and purification of intermediates, and the selectivity of 1,5-PeD was 70 %. A one-step method was proposed by Adkins's team, although this method can make the THFA direct to 1,5-PeD; however, the selectivity of 1,5-PeD was only 20 %, with 1,2-PeD as the main product [35]. In addition, some other authors also report about conversion of THFA to 1,5-pentanediol (1,5-PeD) [36–40]. In this paper, our team mainly discussed that THFA can be obtained by selective hydrogenation of FA in liquid phase (Scheme 1).

Some works have been done in catalytic conversion of FA to THFA. Winterle et al. [41] and Tike et al. [42] have found that FA can be converted to THFA with noble-catalysts (Pd, Pt and Rh) and has a high conversion and selectivity. The selectivity toward THFA was over 97 % below 333 K with 0.68–4.08 MPa reaction pressure. Considering the high price of noble-metals, Chen et al. [43] have used a series of support Ni catalysts for catalytic hydrogenation of FA to THFA with a reaction temperature within 433–453 K, reaction pressure 3–4 MPa, reaction time of 8 h, and catalyst loading 20 g/L. The conversion of FA was nearly 99.9 % with a selectivity of 98.3 % toward THFA. However, much work still needs to be done in exploring low-cost catalysts with good catalytic performance under moderate reaction conditions.

Nickel-base catalysts were widely used in hydrogenation, hydrodesulfurization, and steam reforming for its various advantages such as low cost and easy
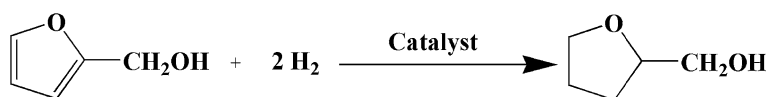
Scheme 1 Possible reaction path for hydrogenation of FA in liquid phase

preparation and high stability [44, 45]. γ-alumina (γ-Al$_2$O$_3$) was confirmed to be a suitable support, owing to its intrinsic properties such as chemical inertness and thermal stability. Due to Ni metal having a facile hydrogen activation, it has been widely recognized as a promising candidate for hydrogenation. Sitthisa et al. [46] reported Ni metal as more favorable for the ring opened products. The Kong et al. [47] team reported that due to the acid sites adjacent to Ni metal, this leading to Ni metal played an important role in the hydrogenation. In addition, in the process of preparation, the high nickel is easily reduced to low nickel in the hydrogenation reaction. All of this illustrates that Ni plays an important role in contributing to the selectivity and conversion of FA and THFA.

In this paper, the impregnation method was chosen to prepare γ-Al$_2$O$_3$-support Ni catalysts, because the deposition–precipitation method was reported to affect the catalytic performance of the metal particles [48]. We found that with the increase of the Ni loading amount, the particle size also increased, and, when the Ni loading amount was 15 wt%, the catalysts showed the best catalytic performance. The catalytic hydrogenation of FA to THFA was improved by high Ni dispersal, which also showed high turnover frequency (TOF) values based on the numerous surface metal sites. A series of nickel-base catalysts were developed for hydrogenation of FA to THFA, mainly focusing on the reaction time, reaction temperature, nickel loading amount, and solvent and hydrogen pressure on conversion of furfural alcohol and selectivity for tetrahydrofurfuryl alcohol. In comparison with previous work [43], it was found that the catalyst we adopted allowed a much lower reaction temperature (353 K) and shorter reaction time (2 h) with satisfactory conversion and selectivity, which could not only save energy greatly, but also improve environmental quality.

Experimental

Chemicals and equipment

FA, alcohol, methanol, Ni(NO$_3$)$_2$·6H$_2$O, and γ-alumina particles were all purchased from the local Sinopharm Chemical Reagent (purity more than 98 %), which were directly used without further treatment.

Catalyst preparation

γ-alumina particles were pretreated by mall bills and calcined at 673 K for 4 h. Then, 10 g γ-alumina and a certain amount of Ni(NO$_3$)$_2$·6H$_2$O were added into 200 mL deionized water and stirred for 24 h at room temperature. The mixture was dried at 393 K for 12 h and calcined at 673 K for 4 h subsequently. Then, a nickel-based catalyst was obtained after reduction in H$_2$ at 623 K for 4 h.

Catalyst characterization

The prepared nickel-based catalyst was characterized by powder X-ray diffraction (XRD) which measurement performed on a Rigaku D/max-A instrument with a Cu Kα radiation at 40 kV and 20 mA and a scan speed of 0.02 °C/min.

The structure of the catalyst was examined with a scanning electron microscope (SEM).

The catalyst with transmission electron microscopy (TEM) analysis was performed on a JEM-2100 instrument. The samples were prepared by mortar and a droplet of ethanol to dilute the samples, then ultrasonically treated for 2 h make the sample disperse completely.

The catalyst for X-ray photoelectron spectroscopy (XPS) analysis was performed on a ESCALAB250Xi instrument. For in situ XPS analysis, the catalyst was placed inside the XPS chamber and heated to 550 °C in the presence of 0.15 mbar H_2 pressure. The temperatures were kept constant for 2 h in 550 °C under 0.15 mbar H_2 pressure prior to recording. The XPS spectra were recorded at a pass energy of 60 eV.

Fifty milligrams of catalyst was processed in the quart tube reactor by H_2 temperature-programmed reduction (H_2-TPR TP-5076), then it was pretreated in helium (40 mL/min) at 400 °C for 1 h. After cooling to 100 °C, the sample was heated from 50 to 800 °C at a heating rate of 30 °C/min in H_2 (40 mL/min).

The catalyst of H_2-chemisorption analysis was conducted on the same apparatus as H_2-TPR (TP-5076). The step is the same as the H_2-TPR, when cooled to 100 °C, hydrogen (40 mL/min) pulses were poured into the helium stream to make the effluent area of consecutive pulses constant.

The BET surface was carried out on the Brunauer-Emmett-Teller (BET 3H-2000PS1).

Catalytic hydrogenation of FA

Before the reaction, the catalysts were reduced by H_2 in the tube furnace. After reduction, the catalysts were still kept in the tube avoiding oxidation of catalysts' surfaces in case of exposure to air. The surface oxidation can affect the catalytic performance. When the reaction began, we took plastic wrap to protect the catalyst and quickly added the catalysts into the reaction equipment. In this process, we usually spent a minute or two. During the reaction, we also found that when the catalyst exposure to air was for 5 min, it did not have any effect on the reaction. All the liquid-phase catalytic hydrogenation of FA was carried out in a 100 mL stainless autoclave equipped with an electromagnetically driven stirrer. For each run, 42.5 g alcohol, 7.5 g FA, and 1 g catalyst were added to the reactor vessel. After displacing the air, the hydrogen pressure was raised to a certain value. Then the reactor was heated to the desired temperature, and the stirring speed was fixed at 600–800 rpm to eliminate diffusion effects [49]. The hydrogenation reaction was carried out in a reaction time range of 2–10 h to estimate the effect of reaction time. Meanwhile the reaction was carried out between 353 and 423 K to estimate the effect of reaction temperature. In addition, other effect factors such as hydrogen pressure, Ni-loading

amount, and solvent were also taken into consideration. When all the operating conditions reached the settings, pressure drop was recorded every 10 min until there was no obvious H_2 pressure drop in a 30 min period. Finally, the reactor was quickly cooled to room temperature, and the product samples were centrifuged to separate the liquid products from the catalyst particles. The liquid phase was analyzed by gas chromatography (Ouhua GC-9160) equipped with an SE-54 capillary column (30 m × 0.32 mm × 0.5 μm), with a flame ionization detector (FID). The vaporization temperature was 473 K, the detector temperature was 473 K, and the oven temperature was 403 K. The main product was THFA, and the product yield and selectivity were calculated and defined as follows:

$$X_{FA} = \frac{n_{FA}^0 - n_{FA}}{n_{FA}^0} \times 100\,\%,$$

$$y_i = \frac{n_i}{n_{FA}^0} \times 100\,\%,$$

$$S_i = \frac{y_i}{X_{FA}} \times 100\,\%,$$

where i represents the product FA in the reaction; n_{FA}^0 and n_{FA} describe the amounts of FA before and after the reaction, respectively, in mol; and n_i is the amount of product i, in mol.

Results and discussion

Catalyst characterization

Figure 1a shows the XRD patterns of the calcined nickel-based catalyst before reduced by hydrogen with a different Ni loading amount. The peaks at 45.5° and 68.5° could be assigned to the diffraction peaks of the (002), (003) planes of γ-Al_2O_3 (PDF No. 75-921). Three diffraction peaks of NiO at 38.5° (111), 45.5° (200), and 65.5° (220) were found when the Ni loading amount was up to 15 wt%. When the Ni loading amount was below 15 wt%, there was only one peak of NiO at 38.5° (111) observed. The reason for this phenomenon is that the surface of support has little Ni, which cannot be found. Figure 1b shows the XRD patterns of the reduced nickel-based catalyst with different Ni loading amounts. All the samples had the characteristic reflections of Ni and γ-Al_2O_3. The sharp and symmetric peaks clearly indicated that the nickel-based catalysts crystallized well. The peak at 45.5° and 68.5° could be assigned to the diffraction peaks of the (002), (003) planes of γ-Al_2O_3 (PDF No. 75-921). Except for the γ-Al_2O_3 feature, the feature of Ni in the nickel-based catalyst is clearly revealed. As we can see from Fig. 1b, the peak at 38.5° could be assigned to the diffraction peak of the (111) planes of Ni (PDF No. 47-1049). The curve of 15 wt% Ni/γ-Al_2O_3 shows more sharp and symmetric peaks than other curves. The reason for this phenomenon is that Ni in the surface of the support has a good crystal shape (Fig. 8). In addition, from the figure, the obvious
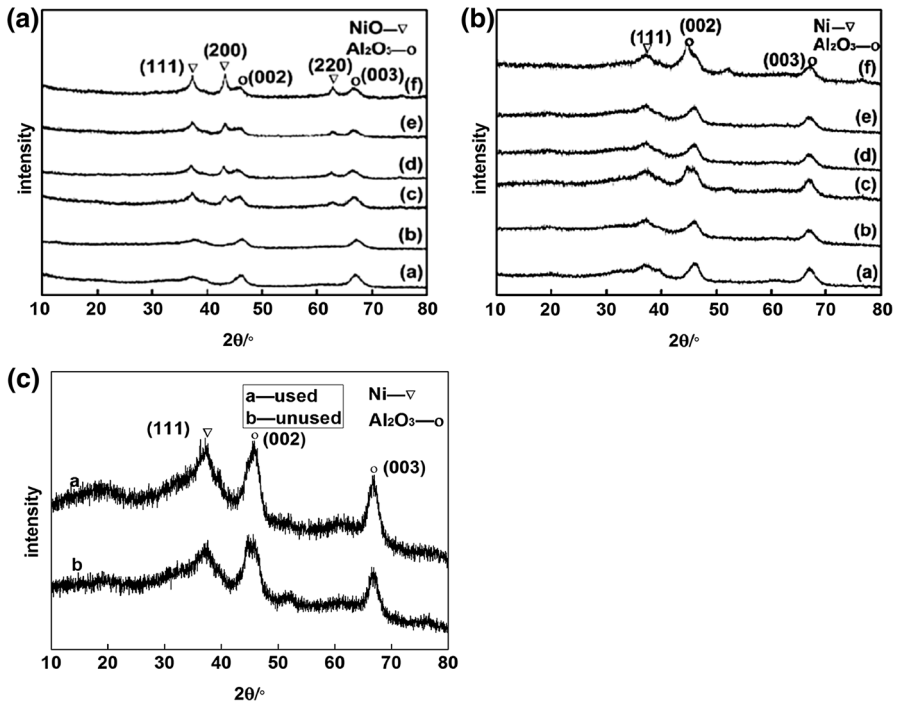
Fig. 1 **a** XRD patterns of nickel-based catalyst with different Ni loading amounts: (*a*) 5 wt% Ni/γ-Al$_2$O$_3$, (*b*) 10 wt% Ni/γ-Al$_2$O$_3$, (*c*) 15 wt% Ni/γ-Al$_2$O$_3$, (*d*) 20 wt% Ni/γ-Al$_2$O$_3$, (*e*) 25 wt% Ni/γ-Al$_2$O$_3$, and (*f*) 30 wt% Ni/γ-Al$_2$O$_3$. **b** XRD patterns of reduced nickel-based catalyst with different Ni loading amounts: (*a*) 5 wt% Ni/γ-Al$_2$O$_3$, (*b*) 10 wt% Ni/γ-Al$_2$O$_3$, (*c*) 15 wt% Ni/γ-Al$_2$O$_3$, (*d*) 20 wt% Ni/γ-Al$_2$O$_3$, (*e*) 25 wt% Ni/γ-Al$_2$O$_3$, and (*f*) 30 wt% Ni/γ-Al$_2$O$_3$. **c** XRD patterns of used catalyst and unused catalyst

difference in Fig. 1a, b is that metal diffraction peak is reduced. In Fig. 1a, there are three different NiO oxide diffraction peaks, however, in Fig. 1b, only the Ni metal diffraction peak existed ascribed to Ni^{2+} that reduced Ni^0 in the tube furnace. From Fig. 1b, there is no NiO oxide diffraction peak, it was determined that the Ni^{2+} was reduced to Ni^0 completely at 623 K. In addition, from the data of XRD, our team also calculated the particle size of Ni (see Table 1) and NiO. When the Ni loading amount is at the low level, the peak of Ni is not clear indicating the good dispersion of Ni. With the increase of Ni loading amounts, the peak of Ni began to become

Table 1 Particle size of NiO and Ni in the calcined and reduced states

Ni-loading amount	Ni particle size (nm)	NiO particle size (nm)
5 wt% Ni/γ-Al$_2$O$_3$	4.9	7.4
10 wt% Ni/γ-Al$_2$O$_3$	4.7	6.5
15 wt% Ni/γ-Al$_2$O$_3$	4.6	5.6
20 wt% Ni/γ-Al$_2$O$_3$	4.3	5.0

The particle size were calculate by XRD

intensive. When the Ni loading amount is up to 15 wt%, the peak of Ni can be detected. It also showed that the 15 wt% nickel-based catalyst contributed to conversion of FA and assured high selectivity toward THFA (Fig. 5). In addition, Fig. 1c shows the XRD patterns of used catalyst and unused catalyst. We can see that the diffraction peaks position of catalyst has not obviously changed in the process of the hydrogenation reaction. The diffraction peaks show intensity enhancement after the nickel based catalyst was used. The reason may be caused by the particle size increase after use (see Fig. 4). In Table 1, we can see that the particle size of NiO and Ni decreased with the increase of nickel loading amounts. Figure 1 shows the diffraction peak of γ-Al_2O_3 is not changed before and after reduction. It can be seen that the support of γ-Al_2O_3 is stable. The diffraction peak of Ni has a large change after the reduction by H_2. When the Ni loading amount is under 15 wt%, the peak of NiO does not appear completely. When the Ni loading amount is up to 15 wt%, the diffraction peak of NiO obviously completely appears.

Figure 2 shows the XPS pattern of the catalyst. Our team analyzed the composition of prepared 15 wt% Ni/γ-Al_2O_3. Absorption peaks were identified for Ni, O and C. Figure 2a shows the general XPS spectra of nickel-based catalyst. It perfectly shows the absorption peak of Ni, O, and C. From Fig. 2b, binding energies at 855.9 and 861.3 eV were observed for nickel-based catalyst, corresponding to Ni^0 ($2p_{3/2}$) and Ni^{2+} ($2p_{3/2}$), respectively. The binding energies at 872.5 and 880.1 eV correspond to the main lines of Ni^0 ($2p_{1/2}$) and Ni^{2+} ($2p_{1/2}$) [50].

The H_2-TPR results are presented in Fig. 3. It can be seen that all the catalysts have a relatively intensive H_2 consumption peak at about 350–400 and 520–570 °C with the increase of Ni loading amount in the catalysts. The peak of 350–400 °C was ascribed to the reduction of bulk NiO oxides in the interaction with Al_2O_3 [51–53]. Meanwhile, the peak of 520–570 °C was ascribed to complex NiO species, which have stronger interaction with the γ-Al_2O_3 support [54]. Manikandan's team and Kong's team also report about NiO species having stronger interaction with Ni-supports [55, 56]. With the increase of Ni-loading amounts, the figure exhibited broad reduction profiles, which could be ascribed to the reduction of NiO species. From the figure, we can see that under 350 °C the profile has no H_2 consumption, and it also shows that the reduction temperature should higher than 350 °C. In addition, our team also studied the impact of reduced temperature on conversion and
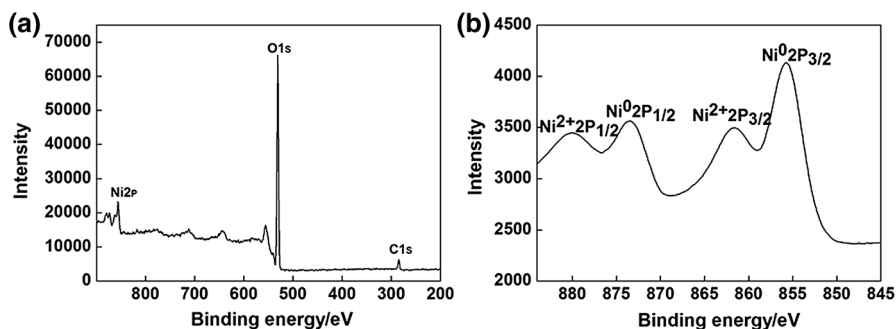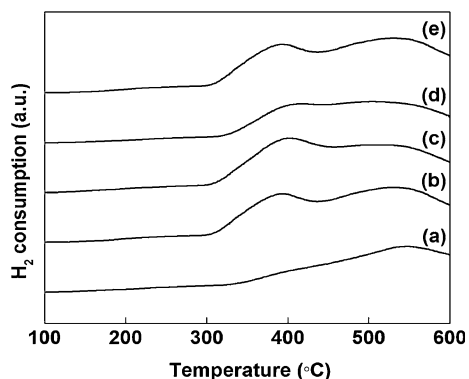

Fig. 2 a General XPS spectra of 15 wt% Ni/γ-Al_2O_3. b XPS pattern of Ni2p of 15 wt% Ni/γ-Al_2O_3

Fig. 3 H$_2$-TPR of Ni/γ-Al$_2$O$_3$ catalysts with different loading amounts: (*a*) 10 wt% Ni/γ-Al$_2$O$_3$, (*b*) 15 wt% Ni/γ-Al$_2$O$_3$, (*c*) 20 wt% Ni/γ-Al$_2$O$_3$, (*d*) 25 wt% Ni/γ-Al$_2$O$_3$, and (*e*) 30 wt% Ni/γ-Al$_2$O$_3$

selectivity (see Table 2). Profile (a) shows that the H$_2$ consumption peak at 350–400 °C is not obviously found due to little of the bulk NiO oxides (Fig. 3). Figure 3 shows that with increase of Ni loading amounts the H$_2$ consumption peak at 350–400 °C can be obviously found. It indicates that the increase of Ni loading amounts in the Ni/γ-Al$_2$O$_3$ catalysts can lead to the increase of bulk NiO species.

Table 3 shows the fundamental physical properties of the nickel-based catalysts, including BET surface area and pore volume. The BET surface areas for the Ni/γ-Al$_2$O$_3$ catalysts range from 163.7 to 188.3 m^2/g concerning the Ni loading amount. From the data, we can make a conclusion that the BET surface area is not considered changed with the change of Ni loading amounts. The Hou et al. [50] team reported that the increase of Ni content in the Ni/γ-Al$_2$O$_3$ catalysts led to the decrease of the BET surface areas. The decreased BET surface area was mainly caused by the coverage of Ni on the γ-Al$_2$O$_3$ surface. In our report, the increase of Ni-loading amount led to a slight change of BET area; therefore, we ignore the impact of area on catalytic activity.

Table 4 shows the particle size of nickel-based catalysts and the reduction degree calculated by three different methods,such as XRD, TEM, and H$_2$ adsorption. The XRD method used Scherrer's equation. The method of H$_2$ adsorption is based on the dispersion and reduction degree. The reduction degree represents that consumed in TPR after decomposition of nitrate. We can see from the picture that the particle size increase from 4.3 to 4.9 nm with the Ni loading amount decreased from 20 to 15 wt%. These particle sizes were smaller than the Montes team's report, the Louis team's report, and the Pilar team's report [48, 57, 58]. In the left column, the reduction degree has almost no change.

Table 2 Effect of reduction temperature on conversion and selectivity

Reduction temperature (°C)	200	250	300	350
Conversion (%)	34.7	50.8	70	99.8
Selectivity (%)	70.4	86.5	99.2	99.5

Reaction conditions: 1 g 15 wt% Ni/γ-Al$_2$O$_3$ catalyst, 42.5 g alcohol, 7.5 g furfuryl alcohol; reaction temperature 353 K; reaction time 2 h; and reaction pressure 4 MPa

Table 3 Physical properties of Ni/γ-Al$_2$O$_3$ catalysts

Catalyst	SBET (m^2/g)	VP (mL/g)
5 wt% Ni/γ-Al$_2$O$_3$	188.3	0.9052
10 wt% Ni/γ-Al$_2$O$_3$	182.4	0.7963
15 wt% Ni/γ-Al$_2$O$_3$	174.4	0.7433
20 wt% Ni/γ-Al$_2$O$_3$	163.7	0.6593

Table 4 Particle size of Ni/γ-Al$_2$O$_3$ catalysts

Catalyst	Reduction degree	H$_2$ adsorption	XRD	TEM
5 wt% Ni/γ-Al$_2$O$_3$	0.9	2.4	4.9	–
10 wt% Ni/γ-Al$_2$O$_3$	1.0	3.5	4.7	–
15 wt% Ni/γ-Al$_2$O$_3$	1.0	4.3	4.6	6.52
20 wt% Ni/γ-Al$_2$O$_3$	0.9	5.7	4.3	–

The H$_2$ adsorption, XRD, and TEM are three different methods to calculate particle size (nm)

Table 5 TOF value of catalysts

Catalyst	TOF	TOF [11]
5 wt% Ni/γ-Al$_2$O$_3$	0.7	–
10 wt% Ni/γ-Al$_2$O$_3$	1.0	–
15 wt% Ni/γ-Al$_2$O$_3$	1.1	0.63
20 wt% Ni/γ-Al$_2$O$_3$	0.9	–

TOF value. Reaction condition: 42.5 g alcohol, 7.5 g furfuryl alcohol; reaction temperature 353 K; reaction time 1 h; reaction pressure 4 MPa

Table 5 shows the TOF values that are calculated by the H$_2$ adsorption amount (Table 4). For the data from the table, we calculated when the catalysts were not in the optimum reaction condition. We adopted the reaction time of 1 h. From the table, we can see that the TOF is similar to the Ni/γ-Al$_2$O$_3$ (Ni loading amount is 5 to 20 wt%) with the Ni particle size 2.4 to 5.7 nm (Table 4). In the right column is the TOF from Yoshinao's team [11]. In the reference, the preparation method of catalyst was different from our team. Our catalyst calcined at 773 K which is similar to the reference; therefore, our team only compared the 15 wt% Ni/γ-Al$_2$O$_3$ with the reference. We can see that our TOF value is larger than the value obtained by Yoshinao's team. Che's team and Shin's team reported that, if the activity is structure-sensitive, the catalytic activity will greatly change when the particle size of the catalysts is in the typical region [59, 60]. Therefore, we also adopt this method in the hydrogenation reaction.

Figure 4 shows the TEM image of nickel-based catalyst (Ni loading amount up to 15 wt%) and reused nickel-based catalyst (Ni loading amount up to 15 wt%). From the picture of (a) and (b), the range of particle size from 4.5 to 6 nm, this result corresponded fairly well with XRD and H$_2$ adsorption. It also verified the particle
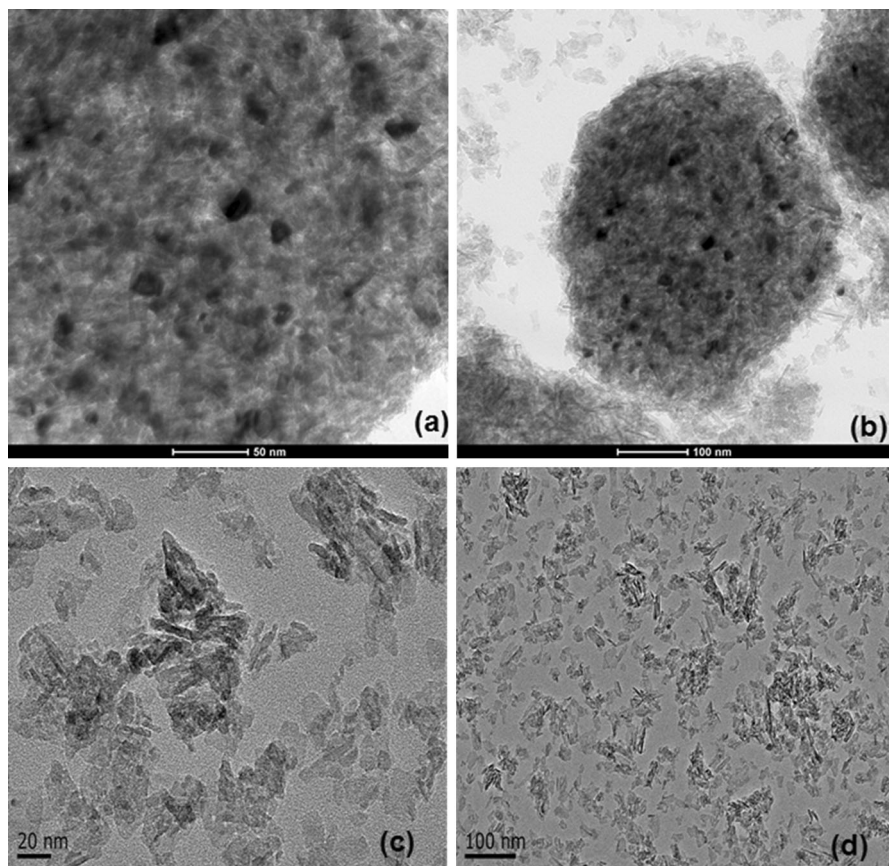
Fig. 4 a, b TEM of Nickel-based catalyst (15 %); c, d TEM of reused Nickel-based catalyst (15 %)

sizes of Ni determined by various methods agreeably well. From the picture of (c) and (d), we can see that it has a large support and that a large number of Ni metal got together. The reason for this is because the reused catalyst lead to Ni metal active component agglomeration. From the picture of (c) and (d), the particle size of the used 15 wt% Ni/γ-Al$_2$O$_3$ catalyst is in the range of 8–11 nm, which is larger than the fresh 15 wt% Ni/γ-Al$_2$O$_3$ catalyst. This indicates that when the agglomeration happened it leads to catalyst activity decreasing. This was the reason that the catalytic activity decreased with the number of used nickel-based catalysts.

Catalytic hydrogenation of furfuryl alcohol

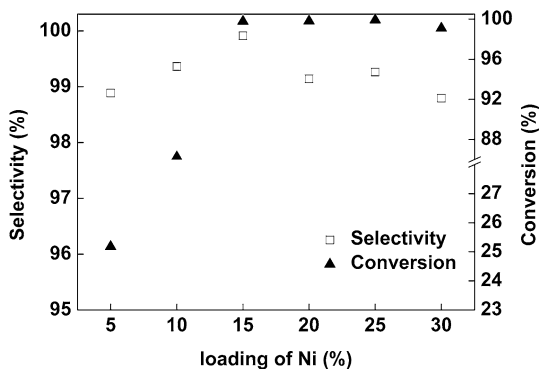*Influence of Ni loading amount on the conversion and selectivity*

First, we show in Table 6 that when the reaction was not carried out at optimum reaction conditions, we adopted 1 h as the reaction time. We found that the

Table 6 Effect of Ni loading amount on conversion and selectivity

| Ni loading	5 %	10 %	15 %	20 %	25 %	30 %
Conversion (%)	10.7	65.2	79.3	80.1	80.9	81.1
Selectivity (%)	65.5	80.7	92.1	93.3	93.9	94.1

Reaction conditions: 42.5 g alcohol, 7.5 g furfuryl alcohol; reaction temperature 353 K; reaction time 1 h; and reaction pressure 4 MPa

Fig. 5 Effect of Ni loading amount on conversion and selectivity. 42.5 g alcohol, 7.5 g furfuryl alcohol; reaction temperature 353 K; reaction time 2 h; and reaction pressure 4 MPa

conversion of FA and selectivity toward THFA increased with the increase of the Ni loading amount. In addition, Fig. 5 shows the effect of Ni loading amounts on the conversion of FA and selectivity toward THFA. As can be seen from Fig. 5, the reaction conversion increases from 25.1 % to about 99.7 % with the increase of Ni loading amounts. The conversion of FA was up to 99.7 % over 15 wt% Ni/γ-Al$_2$O$_3$. When the Ni loading amount continues to increase, the reaction conversion has almost no change. In addition, Fig. 1b shows that 15 wt% Ni/γ-Al$_2$O$_3$ has good dispersibility, which is helpful for increasing the reaction conversion and selectivity. The selectivity toward THFA has a high level no matter what the Ni loading amount (it varied from 5 to 30 wt%). The amount of by-product in this reaction can be ignored, which was very subtle (<0.02 %). The increase of the Ni loading amount could lead to the improvement of FA conversion due to the increase of Ni in the catalysts, from which it could be shown that the diffraction peak Ni (Fig. 1a) is in favour of catalytic hydrogenation of FA. The figure shows that when the Ni loading amount is 5 and 10 wt%, the conversion of FA obviously is lower than 100 %. The reason is the Ni loading amount in the surface of catalysts is very little and it directly lead to catalytic performance. When the Ni loading amount in the low phase, the complex NiO species has little interaction with γ-Al$_2$O$_3$ support. It was also support by the H$_2$-TPR (Fig. 3). So, the optimum loading amount of Ni in Ni/γ-Al$_2$O$_3$ is 15 wt%.

Fig. 6 Effect of reaction temperature on the conversion and selectivity. 1 g 15 wt% Ni/γ-Al₂O₃ catalyst, 42.5 g alcohol, 7.5 g furfuryl alcohol; reaction time 2 h; and reaction pressure 4 MPa
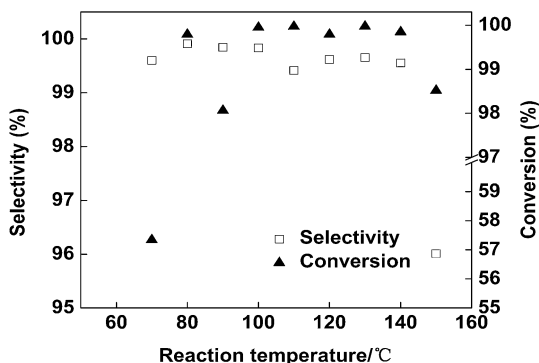
Influence of reaction temperature on conversion and selectivity

Figure 6 shows the influence of the reaction temperature on the conversion of FA and the selectivity of THFA. As can be seen from Fig. 6, the conversion of FA increased from the 57.3 to 99.7 % when the temperature increased from 70 to 150 °C, and the conversion reached a peak at 80 °C (about 99.7 %). Then the conversion has no obvious change with further increase of the temperature. It also can be seen that the selectivity of THFA has almost no change (about 99.5 %) with the change of reaction temperature, which shows that the reaction temperature has little impact on the selectivity of the reaction when the reaction temperature is up to 80 °C. The reaction has almost no by-product when the temperature changes from 80 to 140 °C. When the temperature was higher than 140 °C, dark and viscous compounds began to appear due to the side reactions (such as polymerization) that happened during the reaction. Therefore, considering the energy consumption and the by-product during the reaction, the optimum reaction temperature is selected as 80 °C.

Influence of reaction time on conversion and selectivity

As can be seen in Fig. 7, the reaction time was a great important factor in the catalytic hydrogenation of FA. Obviously, when the reaction time was prolonged, the conversion of FA increased gradually from 63.4 to 99.7 %. However, the selectivity toward THFA had no obvious change when the time ranged from 1 to 10 h. When the reaction was carried out for 2 h, the reaction could give both better conversion and selectivity toward the wanted THFA (about 99.5 %). Therefore, 2 h was finally selected as the optimum reaction time.

Influence of hydrogen pressure on conversion and selectivity

Figure 8 shows the effect of the hydrogen pressure on the conversion of FA and selectivity toward THFA. As can be seen from Fig. 8, the reaction conversion increases with the increase of hydrogen pressure. When the hydrogen pressure reached 4 MPa, the conversion was up to 99.7 %, but with the further increase of

Fig. 7 Effect of reaction time on conversion and selectivity. 1 g 15 wt% Ni/γ-Al₂O₃ catalyst, 42.5 g alcohol, 7.5 g furfuryl alcohol; reaction temperature 353 K; and reaction pressure 4 Mpa
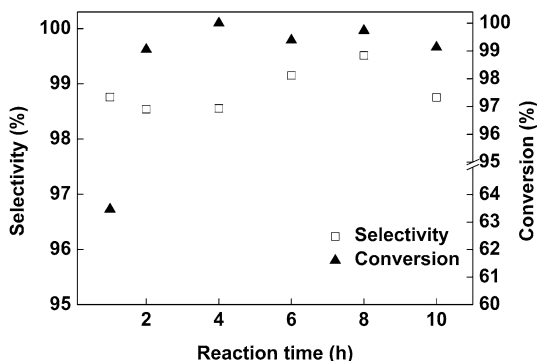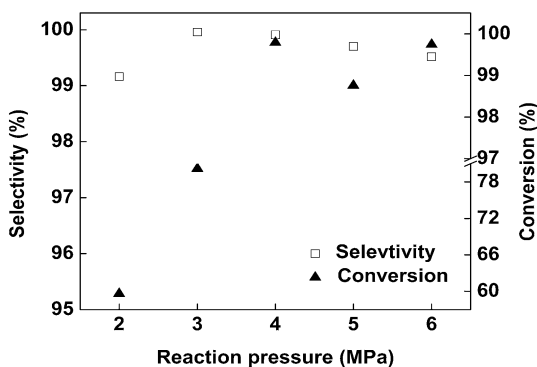

Fig. 8 Effect of reaction pressure on conversion and selectivity. 1 g 15 wt% Ni/γ-Al₂O₃ catalyst, 42.5 g alcohol, 7.5 g furfuryl alcohol; reaction temperature 353 K; and reaction time 2 h

the reaction pressure, there is almost no change in the conversion. The increase of conversion can be explained by the pushing effect of excess hydrogen on the reaction balance as the hydrogen pressure increased from 2 to 4 MPa. However, the selectivity toward THFA was always kept at a high level (about 99.5 %). The results show that the hydrogen pressure has a large impact on the conversion of the reaction and little impact on the selectivity. The optimal hydrogen pressure is 4 MPa.

Influence of solvent on conversion and selectivity

As can be seen in Table 7, the solvent has a great effect on the hydrogenation of FA. It can be seen that when water was used as solvent, the reaction conversion and selectivity had a low level. The conversion of FA is only 51.5 %, the selectivity toward THFA is only 87 %. When ethanol was chosen as the reaction solvent, the reaction conversion and selectivity were up to 99.9 and 99.7 %, respectively. When methanol was selected as the reaction solvent, the selectivity toward the product had a high level, however, the conversion of FA was lower than 99.7 %. The better conversion and selectivity might be caused by the hydrogen-donor effect of ethanol, which has been reported by Ouyang's group [61]. We have also investigated the hydrogen-donor effect of ethanol. In addition, from the price perspective, ethanol is

Table 7 Effect of solvent on the conversion of FA and selectivity toward THFA

Solvent	Selectivity (%)	Conversion (%)
Water	87.0	51.5
Ethanol	99.9	99.7
Methanol	99.7	93.4

Reaction conditions: 1 g 15 wt% Ni/γ-Al$_2$O$_3$ catalyst, 42.5 g alcohol, 7.5 g furfuryl alcohol; reaction temperature 353 K; reaction time 2 h; and reaction pressure 4 MPa

Table 8 Effect of support on the conversion of FA and selectivity toward THFA

Support	Selectivity (%)	Conversion (%)
None	54.1	33.6
γ-Alumina	99.9	99.7

Reaction conditions: 1 g catalyst, 42.5 g alcohol, 7.5 g furfuryl alcohol; reaction temperature 353 K; reaction time 2 h; and reaction pressure 4 MPa

cheaper than methanol and pollution-free for the environment. So, the optimum solvent is ethanol.

Influence of support on the conversion and selectivity

We can see from Table 8 that the support has a great effect on conversion of FA and selectivity toward THFA. In this part, our team mainly investigated the impact of γ-alumina and no support on the hydrogenation of FA. In Table 8, when we chose γ-alumina as support, the conversion and selectivity was up to 99.9 and 99.7 %, respectively. It illustrates that the Ni metal has a stronger interaction with γ-alumina. In addition, when we do not choose any support, we found that the conversion and selectivity were both in the low phase. This illustrates that the support has a great effect on the reaction.

Catalyst recyclability

To study the recyclability of the catalyst, a batch of 15 wt% Ni/γ-Al$_2$O$_3$ was used repeatedly for the catalytic hydrogenation of FA at 353 K in alcohol. All the used catalyst was washed in alcohol then dried at 333 K. It can be seen from Table 9 that the conversion has slightly decreased after the catalyst was reused twice; however, the selectivity toward THFA decreased obviously indicating the decrease of catalyst activity, which might be caused by catalyst agglomeration in the catalytic hydrogenation process of FA (see Fig. 4) [62]. From Fig. 3, we can see that the particle size of catalyst increased after repeated use. In addition, Fig. 9a shows that the catalysts have a good crystal shape before reuse. It was found from Fig. 9b that

Table 9 Results of repeated use of Ni/γ-Al$_2$O$_3$ catalysts

Entry	Selectivity (%)	Conversion (%)
1	97.6	99.7
2	85.2	99.6
3	60.1	98.4

Reaction conditions: Reaction conditions: 1 g 15 wt% Ni/γ-Al$_2$O$_3$ catalyst, 42.5 g alcohol, 7.5 g furfuryl alcohol; reaction temperature 353 K; reaction time 2 h; and reaction pressure 4 MPa
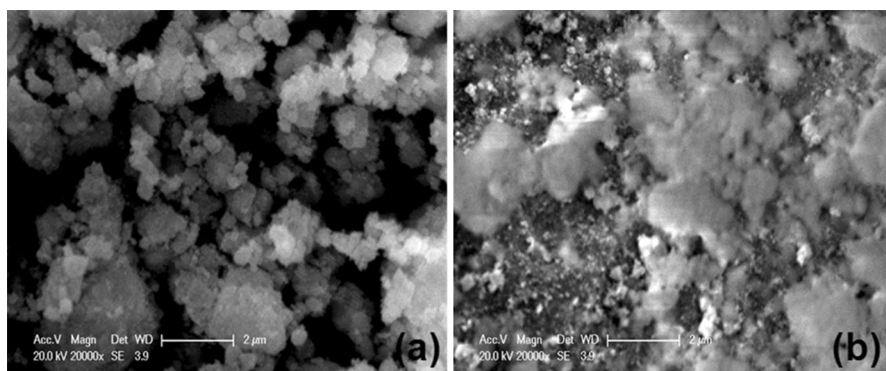

Fig. 9 a SEM of Nickel-based catalyst (15 wt%); **b** SEM of reused oNickel-based catalyst (15 wt%)

we only see large support and a little metal. This can illustrate that the activity component of the catalyst agglomeration phenomenon happened. In addition, our team found that some by-products exist in the reaction when the catalysts were reused twice and for a third time. For example, the main by-products are furan and 2-methylfuran [63]. The reason for this is caused by C=C and C–O bonds rupturing in the hydrogenation reaction. When the catalysts were reused twice, the selectivity toward 2-methyfuran was up to 10 %, and the selectivity toward furan was only 4.3 %. When the catalysts were reused a third time, the selectivity toward 2-methyfuran was up to 30.4 %, and the selectivity toward furan was 9.5 %. As for the reaction, this reaction time of 2 h was selected; prolonged reaction time did not affect the conversion and selectivity in catalyst recyclability.

Conclusion

Ni/γ-Al$_2$O$_3$ catalysts were prepared by the impregnation method and applied in catalytic hydrogenation of furfural alcohol to tetrahydrofurfuryl alcohol. FA could be converted to THFA over 15 wt% Ni/γ-Al$_2$O$_3$ with the yield up to 99.9 % under a reaction temperature of 353 K and reaction pressure of 4 MPa and reaction time of 2 h. The nickel-based catalyst in this reaction has some advantages such as the catalyst's easy preparation, high catalytic activity, and easy separation by simple

centrifugation. The reaction temperature dropped from 433 to 353 K, and reaction time dropped from 8 to 2 h. The experimental results could provide a good research basis for the catalytic preparation of tetrahydrofurfuryl alcohol from furfural alcohol under mild reaction conditions.

References

1. G.W. Huber, S. Iborra, A. Corma, Chem. Rev. **106**, 4044 (2006)
2. P. Gallezot, Chem. Soc. Rev. **41**, 1538 (2012)
3. I. Delidovich, K. Leonhard, R. Palkovits, Energy Environ. Sci. **7**, 2803 (2014)
4. R.A. Sheldon, Green Chem. **16**, 950 (2014)
5. R. Karinen, K. Vilonen, M. Niemela, ChemSusChem **4**, 1002 (2011)
6. L. Hu, G. Zhao, W.W. Hao, X. Tang, Y. Sun, L. Lin, S.J. Liu, RSC Adv. **2**, 11184 (2012)
7. I. Agirrezabal-Telleria, I. Gandarias, P.L. Arias, Catal. Today **234**, 42 (2014)
8. H. Li, Q.Y. Zhang, P.S. Bhadury, S. Yang, Curr. Org. Chem. **18**, 547 (2014)
9. S.P. Teong, G.S. Yi, Y.G. Zhang, Green Chem. **16**, 2015 (2014)
10. R.F. Perez, M.A. Fraga, Green Chem. **16**, 3942 (2014)
11. Y. Nakagawa, H. Nakazawa, H. Watanabe, K. Tomishige, ChemCatChem **4**, 1791–1797 (2012)
12. Y. Nakagawa, K. Tomishige, Catal. Commun. **12**, 154–156 (2010)
13. Y. Nakagawa, K. Takada, M. Tamura, K. Tomishige, ACS Catal. **4**, 2718–2726 (2014)
14. S. Liu, Y. Amada, M. Tamura, Y. Nakagawa, K. Tomishige, Green Chem. **16**, 617–626 (2014)
15. S. Liu, Y. Amada, M. Tamura, Y. Nakagawa, K. Tomishige, Catal. Sci. Technol. **4**, 2535 (2014)
16. R.S. Rao, R.T.K. Baker, M. Vannice, Catal. Lett. **60**, 51 (1999)
17. N. Merat, C. Godawa, A. Gaset, J. Chem. Technol. Biotechnol. **48**, 145 (1990)
18. O. Levenspiel, *Chemical reaction engineering*, vol. 25, 2nd edn. (Wiley, New York, 1972), p. 265
19. A. Corma, S. Iborra, A. Velty, Chem. Rev. **107**, 2411 (2007)
20. N. Merat, C. Godawa, A. Gaset, Chem. Technol. Biotechnol. **48**, 145 (1990)
21. H.P. Thomas, C.L. Wilson, J. Am. Chem. Soc. **73**, 4803 (1951)
22. H.Y. Zheng, Y.L. Zhua, B.T. Teng, Z.Q. Bai, C.H. Zhang, H.W. Xiang, Y.W. Li, Mol J. Catal. A Chem. **246**, 18 (2006)
23. W.H. Bagnall, E.P. Goodings, C.L. Wilson, J. Am. Chem. Soc. **73**, 4794 (1951)
24. E.P. Goodings, C.L. Wilson, J. Am. Chem. Soc. **73**, 4798 (1951)
25. E.P. Goodings, C.L. Wilson, J. Am. Chem. Soc. **73**, 4801 (1951)
26. S. Sato, R. Takahashi, N. Yamamoto, E. Kaneko, H. Inoue, Appl. Catal. A Gen. **334**, 84 (2008)
27. F. Sato, H. Okazaki, S. Sato, Appl. Catal. A Gen. **419**, 41 (2012)
28. E. Sato, S. Sato, Catal. Commun. **27**, 129 (2012)
29. S. Koso, I. Furikado, A. Shimao, T. Miyazawa, K. Kunimori, K. Tomishige, Chem. Commun. **15**, 2035 (2009)
30. S. Koso, N. Ueda, Y. Shinmi, K. Okumura, T. Kizuka, K. Tomishige, J. Catal. **267**, 89–92 (2009)
31. Y. Nakagawa, M. Tamura, K. Tomishige, ACS Catal. **3**, 2655–2668 (2013)
32. Y. Nakagawa, K. Tomishige, Catal. Today **195**, 136–143 (2012)
33. Y. Nakagawa, M. Tamura, K. Tomishige, Catal. Surv. Asia **19**, 249–256 (2015)
34. L.E. Schniepp, H.H. Geller, J. Am. Chem. Soc. **68**, 1646 (1946)
35. H. Adkins, R. Connor, J. Am. Chem. Soc. **53**, 1091 (1931)
36. K. Chen, S. Koso, T. Kubota, Y. Nakagawa, K. Tomishige, ChemCatChem **2**, 547–555 (2010)
37. S. Koso, Y. Nakagawa, K. Tomishige, J. Catal. **280**, 221–229 (2011)
38. S. Koso, H. Watanabe, K. Okumura, Y. Nakagawa, K. Tomishige, Appl. Catal. B Environ. **111–112**, 27–37 (2012)
39. S. Koso, H. Watanabe, K. Okumura, Y. Nakagawa, K. Tomishige, J. Phys. Chem. C **116**, 3079–3090 (2012)

40. B. Aeijelts, G. Mul, M. Makkee, J. Moulijn, J. Catal. **243**, 171–182 (2006)
41. S. Winterle, A. Kraynov, J. Klankermayer, W. Leitner, M.A. Liauw, Chem. Ing. Tech. **82**, 1211 (2010)
42. M.A. Tike, V.V. Mahajani, Ind. Eng. Chem. Res. **46**, 3275 (2007)
43. X.C. Chen, W. Sun, N. Xiao, J.Y. Yan, S.W. Liu, J. Chem. Eng. **126**, 5 (2007)
44. M.V. Rajashekharam, J. Sci. Ind. Res. **56**, 595 (1997)
45. H.R. Reinhoudt, R. Troost, A.D. van Langeveld, J.A.R. van Veen, S.T. Sie, J.A. Moulijn, J. Catal. **203**, 509 (2001)
46. S. Sitthisa, D.E. Resasco, Catal. Lett. **141**, 784–791 (2011)
47. X. Kong, Y. Zhu, H. Zheng, X. Li, Y. Zhu, Y.W. Li, ACS Catal. **5**, 5914 (2015)
48. M.P. GonzalezMarcos, J.I. GutierrezOrtiz, C.G. deElguea, J.A. Delgado, J.R. GonzalezVelasco, Appl. Catal. A **162**, 269–280 (1997)
49. M.H. Zhou, H.Y. Zhu, L. Niu, G.M. Xiao, R. Xiao, Catal. Lett. **144**, 235 (2014)
50. T. Hou, L.X. Yuan, T.Q. Ye, L. Gong, J. Tu, M. Yamamoto, Y. Torimoto, Q.X. Li, Int. J. Hydrogen Energy **34**, 9095 (2009)
51. C. Wu, L. Wang, P.T. Williams, J. Shi, J. Huang, Appl. Catal. B Environ. **108**, 6 (2011)
52. Z. Yuan, L. Wang, J. Wang, S. Xia, P. Chen, Z. Hou, X. Zheng, Appl. Catal. B **101**, 431–440 (2011)
53. C. Rudolf, B. Dragoi, A. Ungureanu, A. Chirieac, S. Royer, A. Nastro, E. Dumitriu, Catal. Sci. Technol. **4**, 179–189 (2014)
54. Z. Hou, O. Yokota, T. Tanaka, T. Yashima, Appl. Catal. A Gen. **253**, 381 (2003)
55. X. Kong, R. Zheng, Y. Zhu, G. Ding, Y. Zhu, Y.W. Li, Green Chem. **17**, 2504–2514 (2015)
56. M. Manikandan, A.K. Venugopal, K. Prabu, R.K. Jha, R. Thirumalaiswamy, J. Mol. Catal. A: Chem. **417**, 153–162 (2016)
57. M. Montes, C.P. deBosscheyde, B.K. Hodnett, F. Delannay, P. Grange, B. Delmon, Appl. Catal. **12**, 309–330 (1984)
58. C. Louis, Z.X. Cheng, M. Che, J. Phys. Chem. **97**, 5703–5712 (1993)
59. M. Che, C.O. Bennett, Adv. Catal. **36**, 55–172 (1989)
60. E.J. Shin, M.A. Keane, Ind. Eng. Chem. Res. **39**, 883–892 (2000)
61. X.P. Ouyang, X.Z. Huang, Y. Zhu, X.Q. Qiu, Energy Fuels **29**, 5835 (2015)
62. H.Y. Zhu, M.H. Zhou, Z. Zou, G.M. Xiao, R. Xiao, Korean J. Chem. Eng. **31**, 593 (2014)
63. S. Bhogeswararao, D. Srinivas, J. Catal. **327**, 65–77 (2015)